

# Impact of anisotropic interactions on non-equilibrium cluster growth at surfaces

Thomas Martynec\* and Sabine H. L. Klapp†

*Institut für Theoretische Physik, Technische Universität Berlin, Hardenbergstr. 36, 10623 Berlin, Germany*

(Dated: December 14, 2024)

Using event-driven kinetic Monte-Carlo simulations we investigate the early stage of non-equilibrium surface growth in systems with anisotropic interactions among the adsorbed particles. Specifically, we consider a two-dimensional lattice model of spherical particles where the interaction anisotropy is characterized by a control parameter  $\eta$  measuring the ratio of interaction energy along the two lattice directions. We systematically study the effect and interplay between interaction anisotropy  $\eta$  and nearest-neighbor interaction energy  $E_n$  on the shapes of growing clusters before coalescence sets in. At finite particle flux  $F$  we observe the emergence of elongated clusters whose elongation depends on  $\eta$  and  $E_n$ . We identify a critical cluster length  $L_c$  that marks a transition from one-dimensional to self-similar two-dimensional cluster growth. Moreover, we find that the cluster properties depend markedly on the critical island size  $i^*$  of the isotropically interacting reference system ( $\eta = 1$ ).

## I. INTRODUCTION

The non-equilibrium surface growth of atomic systems by means of epitaxial layer growth has been intensively studied over the last decades. Several aspects from the sub-monolayer to the multilayer growth regime have been experimentally investigated in detail by atomic force microscopy [1–17], scanning tunneling microscopy [19–22], high or low energy electron diffraction [23–29], Raman [30] and Auger electron spectroscopy [31] experiments. Recently, also X-ray scattering studies of epitaxially grown thin films have been performed [32–34, 36–40]. Furthermore, such purely inorganic systems are theoretically well studied by means of rate equation approaches [46–60] and kinetic Monte Carlo simulations (kMC) [61–64]. Theoretical and numerical results for the island density, island size distribution, evolution of layer coverages and the global interface width are qualitatively in good agreement with experimental data for the growth of certain atomic systems. [46–59]. Moreover, good agreement between experimental data and kMC simulations was also found for the growth of the organic molecule fullerene  $C_{60}$  [32].

The above mentioned observables along with the shape of clusters in the sub-monolayer regime are of peculiar interest regarding the fact that clusters formed in the early stage of thin film growth provide the basis for further nucleation and growth in higher layers. Indeed, depending on properties of initially nucleated clusters, the morphology of the grown structure can drastically vary in the multilayer regime. This may strongly affect mechanical, optical and electrical properties of thin film devices [34, 40].

In the present study we investigate the sub-monolayer growth of systems with anisotropic interactions. However, we note that even spherical atomic systems can exhibit some kind of anisotropy. For example, Cu grown

epitaxially on Pd(110) in the temperature regime below 300 K has revealed a diffusion anisotropy, which is responsible for the formation of one-dimensional clusters [41]. At higher temperatures, transverse diffusion of adsorbed Cu atoms sets in, leading to isotropic diffusion and the formation of regular two-dimensional clusters. Another example is the growth of Ag on fcc metal (110) surfaces: Quenched molecular-dynamics simulations [44, 45] have shown that the energy barriers and interaction energies for in-plane bonds parallel  $[(1\bar{1}0)]$  and normal  $[(001)]$  are not identical, which implies anisotropic interactions among adsorbed atoms. By varying the adsorption rate  $F$  or the substrate temperature  $T$ , a rich variety of cluster morphologies from small isotropic clusters to one-dimensional and elongated two-dimensional clusters is observed [42, 43]. These studies indicate that the ratio  $\Gamma = D_0(T)/F$  of the free diffusion  $D_0(T)$  over adsorption rate  $F$  not only influences the island density (which is well understood [46–48]), but also the cluster morphology. However, details of the interplay between  $\Gamma$  and cluster morphologies in presence of an anisotropy are, so far not well understood.

This is even more the case for systems of conjugated organic molecules (COM). In contrast to most atomic systems or systems of nearly spherical organic molecules like fullerene  $C_{60}$ , elongated organic molecules like diindenoperylene, p-sexyphenyl (6P), the perylene derivative PTCDI- $C_8$  or pentacene are known to generally interact anisotropically with each other when adsorbed on both, organic and inorganic substrates [34, 37, 39, 40, 65–70]. Therefore one expects rather complex cluster shapes and corresponding changes in the island density, island size distribution and the coalescence behavior in the sub-monolayer growth regime as compared to atomic systems. But also when we tend towards multilayer growth, the behavior of organic and hybrid inorganic-organic systems (HIOS) can strongly differ from isotropically interacting systems.

The structural and chemical flexibility of organic molecules is one of the main reasons for the production of hybrid inorganic-organic thin film devices. For exam-

\* martynec@tu-berlin.de

† klapp@physik.tu-berlin.de

ple, the partial fluorinated derivative 6P-F<sub>4</sub> of the prototypical organic semiconductor *para*-sexiphenyl 6P is known to grow in a distinctly different morphology than 6P on the non-polar ZnO(10 $\bar{1}$ 0) surface [34]. For 6P, needle-shaped islands of flat lying molecules are found in the second layer. In contrast to this, fluorinated 6P-F<sub>4</sub> grows in an upright standing fashion with smoother surface morphology than 6P. These examples show the impact of small chemical variations, which change the anisotropic particle-particle and particle-substrate interactions, on the growth mode.

In order to get a deeper insight in how anisotropic interactions affect the non-equilibrium surface growth, we here study the sub-monolayer growth by means of event-driven kMC simulations [88, 89] involving spherical particles with anisotropic nearest-neighbor interactions. The simulations are performed on a two-dimensional square lattice. Particles are adsorbed on the lattice at rate  $F$  and hop between nearest-neighbor sites until they meet other particles, yielding in-plane bonds that reduce the hopping rate. We vary the interaction energy and the degree of anisotropy of bonds to study the effect of modified interparticle interactions on structurally altered organic molecules to mimic effects like different polarities. Thereby, the effect of interaction anisotropy on the shapes of clusters formed in the very early stage of thin film growth is analyzed in detail.

The rest of the paper is organized as follows. In Sec. II A, we describe the event-driven kMC simulation setup and the growth model with anisotropic interactions. In addition, we introduce in Sec. II B an anisotropic version of the Eden growth model. Numerical results for cluster properties for different system settings under non-equilibrium growth conditions are presented in Sec. III. We close with a brief summary and conclusions in Sec. IV.

## II. MODEL AND METHODS

### A. The kMC model with anisotropic interactions

During the non-equilibrium growth process simulated by a kMC algorithm, particles are adsorbed on an initially empty square lattice with an effective adsorption rate  $F$  given in monolayer per minute (ML/min). Once adsorbed, they perform activated Arrhenius-type hopping processes to a randomly chosen nearest-neighbor lattice site. The hopping rate  $r_{ij} \sim \exp(-\beta\Delta E)$  from lattice site  $i$  to a neighboring site  $j$  is determined by an activation energy barrier  $\Delta E$  which involves up to three contributions: (I) an in-plane diffusion barrier  $E_d$ , (II) an additional out-of-plane diffusion barrier for hopping across step-edges  $E_{es}$ , and (III) a nearest-neighbor interaction energy contribution  $E_n$ . In systems with isotropic nearest-neighbor interactions, the corresponding energy contribution (III) depends on the interaction energy  $E_n$  of a two particle bond and on the number

$n = \sum_{\langle ij \rangle} o_{ij}$  of occupied in-plane nearest-neighbor lattice sites (where  $o_{ij} = 0$  if the neighboring site  $j$  is unoccupied and  $o_{ij} = 1$  if  $j$  is occupied). The total contribution of the interaction energy to the hopping rate  $r_{ij}$  then reads  $\sum_{\langle ij \rangle} o_{ij} E_n = n E_n$ . Here we consider anisotropic nearest-neighbor interactions, where not only the number  $n$  of in-plane bonds, but also their configuration matters.

To this end, we define the interaction anisotropy parameter  $\eta \in [0, 1]$  which changes the nearest-neighbor interaction energy of in-plane bonds along the y-axis ( $E_n^y = \eta E_n$ ) relative to that along the x-axis ( $E_n^x = E_n$ ). Thereby, we model generic properties of anisotropic interactions (which are essentially omnipresent for conjugated organic molecules) combined with a global symmetry breaking e.g., an external electric field. Possible candidate systems might be organic oligomers on the (10 $\bar{1}$ 0) surface of a ZnO semiconductor which possesses a periodic dipolar field that induces dipole moments in the adsorbed molecules along the field direction [35]. To give a further example, a dipole moment can be generated by partial fluorination of a conjugated organic molecule like di-fluorinated *para*-sexiphenyl (6P-F<sub>2</sub>) [34]. In our model, setting  $\eta = -1/8$  mimics the interaction of parallel aligned neighboring dipoles.

One important peculiarity of our system is the fact that the particle shape remains isotropic. This allows us to study the impact of anisotropy in the interactions alone, without accounting for steric effects. Clearly, the latter effects are ubiquitous in realistic anisotropic systems such as films of organic systems. However, from the simulation perspective, anisotropic particle shapes lead to additional complications such as blocked pathways for hopping processes, overhangs of adsorbed particles and the difficult question how the out-of-plane diffusion of anisotropically shaped particles should be treated [69, 84–87]. We consider the present simplified model as a first step to the overall goal to better understand the effect of anisotropic interparticle interactions under non-equilibrium growth conditions.

An illustration of the kMC model setup is shown in Fig. 1. The total interaction energy of a particle at site  $i$  reads  $(n_x + \eta n_y) E_n$ , where  $n_x$  is the number of occupied lateral neighbor sites along the x-direction, while  $n_y$  is the same for the y-direction. For  $\eta = 1$ , the model thus reduces to the isotropic case [with total interaction energy  $(n_x + n_y) E_n = n E_n$ , while  $\eta < 1$  represents the situation with anisotropic interactions among the adsorbed particles. Specifically, decreasing  $\eta$  leads to an increase of the anisotropy of interparticle interactions. The resulting expression for the hopping rate from an initially occupied site  $i$  to the final site  $j$  is given by the Clarke-Vvedensky bond-counting Ansatz [88, 89],

$$r_{ij} = \nu_0 \exp\{-\beta [(n_x + \eta n_y) E_n + E_d + s_{ij} E_{es}]\}. \quad (1)$$

Here, we have introduced the attempt frequency  $\nu_0 = 2k_B T/h$ , where  $k_B$  is the Boltzmann's constant,  $T$  the

substrate temperature and  $h$  the Planck constant. Further,  $\beta = 1/k_B T$ . The first term in the exponent  $[(n_x + \eta n_y)E_n]$  describes the contribution to the total activation energy barrier  $\Delta E$  that stems from in-plane interparticle bonds, while the second and third term represent the in-plane ( $E_d$ ) and out-of-plane diffusion barrier ( $E_{es}$ ), respectively. The latter leads to a reduced rate for diffusion processes across step-edges (where  $s_{ij} = 1$ ) by a factor  $\alpha = \exp(-\beta E_{es})$ . The case  $s_{ij} = 0$  corresponds to pure in-plane diffusion.

The simulation consists of a sequence of iterations. After each iteration step, where either a particle performed a hopping process to a randomly chosen nearest-neighbor lattice site or a new particle got adsorbed, the simulation time is updated in a stochastic manner by a time step  $\tau$ . The latter is calculated according to

$$\tau = -\frac{\ln(R)}{r_{\text{all}}}, \quad (2)$$

where  $R \in (0, 1]$  is a random number which is chosen uniformly from the given interval and  $r_{\text{all}}$  is the sum of rates related to all particles adsorbed in the topmost layer on the surface. In other words,

$$r_{\text{all}} = \sum_{i=1}^L \left( \sum_{j=1}^4 r_{ij} + F \right), \quad (3)$$

where  $L$  is the lateral length of the discretized simulation box. Following earlier studies [61–64], we do not allow the collective diffusion of clusters and forbid overhangs and vacancies in the simulations. This means that the solid-on-solid (SOS) condition is applied to the system.

For all simulations in this work, we set the energy barrier for free diffusion to  $E_d = 0.5$  eV. We choose this value because it is a good approximation for several real systems ranging from organic molecules like  $C_{60}$  to inorganic systems like Ag or Pt [32, 61]. The out-of-plane diffusion barrier is set to  $E_{es} = 0.1$  eV for the same reason. The adsorption rate is fixed to  $F = 1$  ML/min and the temperature is set to  $T = 313$  K which is a commonly used temperature in experimental growth studies with organic molecules [18, 32]. If not stated otherwise, the coverage is set to  $\theta = 0.05$ . This low coverage is chosen to make sure that coalescence of clusters has not yet set in. The simulations are performed at different values of the interaction energy and the anisotropy parameter in the ranges  $E_n \in [0.10 - 3.0]$  eV and  $\eta \in [0, 1]$ , respectively. By this we study the interplay between  $E_n$  and  $\eta$  concerning properties of growing clusters in the submonolayer growth regime when anisotropic interactions are present.

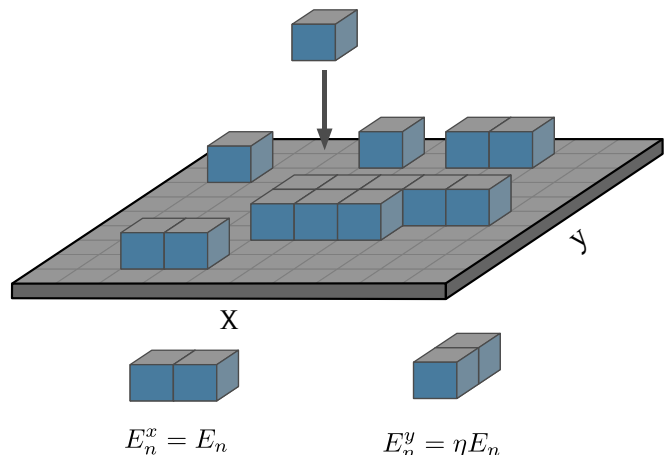


FIG. 1. (Color online) Illustration of our model system for the non-equilibrium cluster formation and lateral growth in presence of anisotropic interactions. The in-plane interaction between particles on nearest-neighbor sites in x-direction is denoted by  $E_n^x = E_n$ . The parameter  $\eta$  controls the degree of interaction anisotropy. For  $\eta = 1$  interactions are isotropic, while for  $\eta < 1$ , the interaction energy  $E_n^y = \eta E_n$  of bonds in y-direction is lowered relative to  $E_n^x$ .

## B. Anisotropic Eden growth model

The kinetic Monte-Carlo algorithm described in Sec. II. A. mimics the kinetically driven growth of thin films based on Arrhenius-type activation energy-dependent process rates. One goal of the present study is to compare the kMC results with those from an anisotropic stochastic Eden growth model. The latter is more elementary in the sense that it simulates cluster growth simply by attachment of particles to an existing cluster. This implies essentially the neglect of computationally costly hopping processes that usually dominate in kMC simulations, especially under realistic growth conditions [77–83].

Within the Eden model, a cluster on the discretized two dimensional lattice space  $\mathbb{L}^2$  is defined as a finite subset  $C \in \mathbb{L}^2$  of occupied lattice sites. At the boundary of such a cluster, unoccupied sites  $\partial C$  that possess at least one occupied neighbor site

$$\partial C = \{j \in \mathbb{Z}^2 \setminus C : \exists i \in C \rightarrow \|i - j\| = 1\}, \quad (4)$$

represent the set of growth sites which have a non-zero probability to be occupied in an iteration step during the cluster growth process. On a square lattice there exist four different types of nodes  $\partial_k C$  ( $k = 1, 2, 3, 4$ ), where  $k$  is the number of occupied neighbor sites. Therefore, the total boundary is simply given by  $\partial C = \partial_1 C \cup \partial_2 C \cup \partial_3 C \cup \partial_4 C$ .

The cluster at initial time  $t_0 = 0$  is a fixed connected set  $C_0 \subset \mathbb{Z}^2$ . In our case, the initial cluster at  $t_0$  consists of just a single occupied site in the middle of the lattice. Thus, there exist four growth sites in the first iteration

step. In each step  $t_n \rightarrow t_{n+1}$  one of the growth sites  $\partial C$  is occupied and the cluster grows  $C_n \rightarrow C_{n+1}$  by one lattice site. The probability  $p_i$  for particle attachment at boundary site  $i$  depends on its local environment, namely the number of occupied nearest-neighbor sites  $s^{nn}$

$$p_i = \sum_{\langle i,j \rangle} s_j^{nn}, \quad (5)$$

where  $s_j^{nn} = 1$  if the neighboring site is occupied,  $s_j^{nn} = 0$  for unoccupied neighbor sites, and the sum  $\langle i, j \rangle$  is taken over all nearest-neighbors of site  $i$ . Therefore, only growth sites with at least one neighboring cluster site have a non-zero probability  $p_i$  to be occupied during the cluster growth process.

In order to model anisotropic interactions, we split the occupation probability  $p_i$  for lattice site  $i$  into two contributions related to the x- and y-direction and impose an imbalance between these two directions. The anisotropy parameter  $\xi$  determines the reduced attachment probability for particles along the y-direction [79]

$$p_i = p_i^x + p_i^y = \sum_{\langle i,j \rangle^x} s_j^{nn} + \xi \sum_{\langle i,j \rangle^y} s_j^{nn}. \quad (6)$$

Here,  $\langle i, j \rangle^x$  denotes occupied neighbors along the x-direction and  $\langle i, j \rangle^y$  along the y-direction. Consequently,  $p_i^y < p_i^x$ , if  $\xi < 1$ . We normalize all probabilities  $\tilde{p}_i = p_i / \sum_{j=1}^c p_j$  such that  $\sum \tilde{p}_i = 1$ . The attachment anisotropy in the stochastic Eden model mimics the interaction anisotropy in the kMC simulations and it results in the formation of elongated clusters for  $\xi < 1$  [79].

The actual simulation proceeds as follows. In each iteration step, we pick a random number  $r \in [0, 1]$  from a uniform interval. If  $r \in [\tilde{p}_i, \tilde{p}_{i+1}]$  we choose site  $i$  to be occupied in this step. Different values for  $\xi$  are used to study the effect of anisotropic interactions on the growth of clusters. The results are compared to clusters from the kMC simulations to check whether this minimal model is able to produce clusters with the same properties.

### C. Target quantities

#### 1. Island shape properties

In order to study how anisotropy in the interparticle interaction affects the shape of growing clusters, we calculate the average length  $L$  of clusters in x-direction as function of cluster size  $S$ . The latter is the number of particles a cluster consists of. We further calculate the extension of the cluster in y-direction, i.e. the cluster width  $W$ . This also yields the aspect ratio  $R = L/W$  which we calculate for different cluster sizes  $S$  as function of interaction energy  $E_n \in [0.10, 3.0]$  eV and anisotropy parameter  $\eta \in [0, 1]$ . The obtained results are averaged

over at least 1000 clusters for each cluster size  $S$ . Furthermore, we calculate the island size distribution  $P(S)$  and the distribution of cluster lengths  $P(L)$  in order to analyze not only average quantities, but also fluctuations around the average.

#### 2. Island density

A further important quantity is the island density  $\rho_N = N/L^2$  (where  $N$  is the number of "stable" islands in the system of size  $L^2$ ) for different values of the interaction energy  $E_n$  and the anisotropy parameter  $\eta$ . Clusters are considered as stable when they grow during the simulation time by subsequent particle attachment rather than dissolve into individual particles again. The latter are called unstable clusters. The distinction between these two types of clusters is typically associated with the critical island size  $i^*$  which is defined as the largest size of unstable clusters such that clusters of size  $S \leq i^*$  dissolve while clusters of size  $S > i^*$  grow. In the early stage of growth, the number of stable clusters, and thus, the island density  $\rho_N$  increases until it saturates at  $\rho_N^c$ . This maximum value of the island density is referred to as the critical island density  $\rho_N^c$ . According to a rate equation approach [57, 71],  $\rho_N^c$  is connected to the critical island size  $i^*$  via the scaling relation  $\rho_N^c \sim (D_0(T)/F)^{-\chi}$ , with the exponent  $\chi = i^*/(i^* + 2)$ , the rate for free in-plane diffusion  $D_0(T) = \nu_0 \exp(-\beta E_d)$  and the adsorption rate  $F$ . We are particularly interested in the critical island size of the systems with isotropic interactions ( $\eta = 1$ ) for different interaction energies  $E_n$ . We take these isotropic systems as "reference" systems because, as will be shown in Sec. III. C, the precise value of  $i^*$  in these systems has strong impact on the cluster shape properties in presence of anisotropic interactions when the nearest-neighbor bond strength in y-direction is reduced to  $E_n^y = \eta E_n$  ( $\eta < 1$ ).

#### 3. The critical island size, reversible versus irreversible cluster growth

The general procedure to determine  $i^*$  for the isotropically interacting reference systems is as follows. First,  $\rho_N^c$  is calculated for different  $\Gamma = D_0(T)/F$  by changing the temperature  $T$ . We then choose  $i^*$  such that it fits the numerically obtained scaling of the critical island density  $\rho_N^c$ . For  $i^* = 1$  ( $\chi = 1/3$ ), already dimers represent stable clusters which do not decay. In this case, the critical island density scales as  $\rho_N^c \sim \Gamma^{-1/3}$ . In other words, the case  $i^* = 1$  corresponds to *irreversible* attachment, where particles become immediately immobilized for the rest of the growth procedure once they form at least one in-plane bond to a neighboring particle. In contrast to this, for  $i^* > 1$  particle attachment is *reversible* in the sense that they may detach from clusters, diffuse further and attach again to the same or some other cluster in

the system. In this case  $\chi < 1/3$ , and consequently  $\rho_N^c$  scales differently compared to the situation  $i^* = 1$ . A major problem with this procedure is that we need to perform simulations at different  $\Gamma$  to obtain the best fit for the scaling of  $\rho_N^c$  that determines  $i^*$  when  $T$ , or  $F$  are varied. However, often we are interested only in the question whether cluster growth is *reversible* or *irreversible* at a specific value of  $\Gamma$ .

As an estimate, we calculate the sum of all hopping events at all time steps  $t_0, t_1, t_2, \dots, t_{f-1}, t_f$  [with  $t_{n+1} = t_n + \tau$  (see Eq. 2)] of the simulation. In this time series  $t_0 = 0$  corresponds to the empty lattice at the start of the simulation, while  $t_f$  corresponds to the time at the end of the simulation when the final coverage of  $\theta = 0.05$  has been reached. In each iteration step  $t_n \rightarrow t_{n+1}$ , where a particle performs a hopping event, we distinguish between free hopping without lateral neighbors ( $n = 0$ ) corresponding to a rate  $r_{ij} \sim \exp(-\beta E_d)$  (denoted as  $r^0$ ) and hopping processes of particles with at least one in-plane bond ( $n > 0$ ) with rate  $r_{ij} \sim \exp(-\beta E_d + n E_n)$  (denoted as  $r^{>0}$ ). We then calculate the sum  $R_0$  of all hopping events with  $r^0$  and the sum  $R_{>0}$  of all events with  $r^{>0}$  during the entire simulation, that is,

$$R_0 = \sum_{t=t_0}^{t_f} r^0(t), \quad r^0(t) = \begin{cases} 1, & n_t = 0 \\ 0, & n_t > 0 \end{cases} \quad (7)$$

$$R_{>0} = \sum_{t=t_0}^{t_f} r^{>0}(t), \quad r^{>0}(t) = \begin{cases} 1, & n_t > 0 \\ 0, & n_t = 0. \end{cases} \quad (8)$$

Here,  $n_t$  is the number of in-plane bonds of the particle that performed a hopping process at time  $t_n$ . From these two sums, we calculate the quantity

$$\omega_1 = \frac{R_0}{R_{>0}}, \quad (9)$$

measuring the ratio between free hopping events and hopping events with in-plane bonds. If cluster growth is *irreversible* ( $i^* = 1$ ), no detachment events occur. Thus,  $R_{>0} = 0$  and consequently  $\omega_1 = 0$ . In contrast, non-zero values of  $\omega_1$  ( $R_{>0} > 0$ ) indicate the presence of detachment events or, in turn, *reversible* cluster growth ( $i^* > 1$ ). This method does not allow a precise determination of the exact value of  $i^*$ , but it is sufficient to distinguish between the cases  $i^* = 1$  and  $i^* > 1$ . We will use the quantity  $\omega_1$  in Sec. III. C to differentiate between *irreversible* or *reversible* cluster growth conditions in the isotropically interacting reference systems.

### III. RESULTS

In the following, we present numerical results of kMC simulations for the non-equilibrium surface growth with

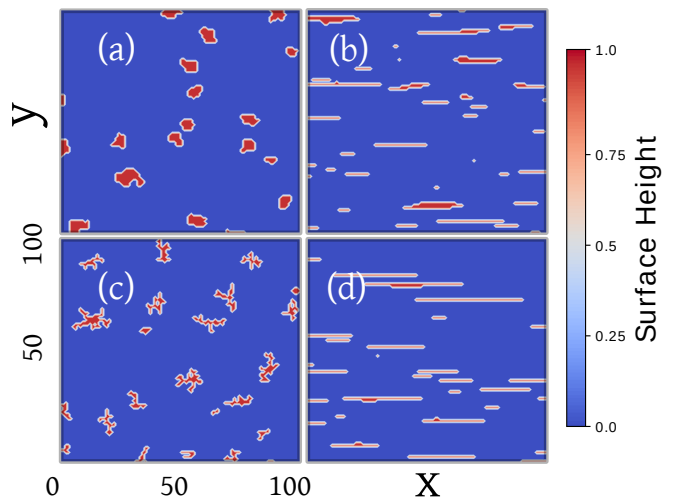


FIG. 2. (Color online) Spatial configurations at coverage  $\theta = 0.05$ ,  $T = 313$  K,  $F = 1$  ML/min (used in all figures). In (a) and (b) the interaction energy is  $E_n = 0.2$  eV. In (a) the interactions are isotropic ( $\eta = 1$ ) while in (b) strong anisotropy in the inter-particle interaction is present ( $\eta = 0.1$ ). The configurations in (c) and (d) depict the same, but at higher interaction energy  $E_n = 0.7$  eV.

interaction energies ranging from  $E_n = 0.10$  eV to  $E_n = 3.0$  eV and interaction anisotropies  $\eta \in [0, 1]$ . First, we mainly focus on two exemplary interaction energies and values of the anisotropy parameter. These are  $E_n = 0.2$  eV and  $E_n = 0.7$  eV and  $\eta = 1$  (isotropic interactions) as well as  $\eta = 0.1$  (strongly anisotropic interactions). We chose these two values of  $E_n$  because, for isotropic interactions,  $E_n = 0.7$  eV represents a reference system with  $i^* = 1$ , while at  $E_n = 0.2$  eV, we find  $i^* = 2$  from scaling of the critical island density  $\rho_N^c$ . Therefore, for  $\eta = 1$  these two values of  $E_n$  represent growth conditions with *reversible* and particle *irreversible* attachment, respectively.

#### A. Spatial configurations and cluster shapes

##### 1. Spatial configurations and distributions

As a starting point, we present snapshots of spatial configurations of surface structures in the sub-monolayer growth regime at coverage  $\theta = 0.05$  ML in Fig. 2 for two interaction energies,  $E_n = 0.2$  [Fig. 2(a) and (b)] and  $E_n = 0.7$  [see Fig. 2(c) and (d)] eV for isotropic ( $\eta = 1$ ) and strongly anisotropic ( $\eta = 0.1$ ) growth conditions at  $T = 313$  K and  $F = 1$  ML/min.

For isotropic growth conditions ( $\eta = 1$ ) the clusters have compact shapes at  $E_n = 0.2$  eV [see Fig. 2(a)], while they are strongly ramified for the much stronger interaction energy  $E_n = 0.7$  eV [see Fig. 2(c)]. This can be explained via corresponding values of the critical island size  $i^*$ . At  $E_n = 0.2$  eV, we find  $i^* = 2$

( $\chi = 1/2$ ). This implies *reversible* attachment, i.e., particles are able to detach from clusters when having only one lateral bond in order to attach to cluster boundary sites with higher coordination number (number of occupied in-plane nearest-neighbor lattice sites). Consequently, this particle rearrangement procedure leads to compact clusters with fractal dimension  $D_f \approx 2$ . We have determined  $D_f$  via a scaling plot of the island area as function of the radius of gyration [61]. At  $E_n = 0.7$  eV, attachment of particles to clusters is *irreversible* ( $i^* = 1$ ,  $\chi = 1/3$ ). This leads to ramified cluster shapes [see Fig. 2(c)] where already one lateral bond is strong enough to suppress particle detachment. Specifically, we find that the fractal dimension in this case is  $D_f \approx 1.7$  which is close to the results for clusters from Diffusion Limited Aggregation (DLA) simulations [72–76].

We observe that strong interaction anisotropy ( $\eta = 0.1$ ) leads to a visible elongation of clusters in x-direction (direction of strong interparticle bonds) for both considered values of  $E_n$ . Moreover, we find that clusters at  $E_n = 0.7$  eV are stronger elongated and have a smaller width  $W$  compared to clusters at  $E_n = 0.2$  eV. This already suggests stronger impact of interaction anisotropy on cluster shape properties at higher interaction energy  $E_n$ . Further, strong interaction anisotropy ( $\eta = 0.1$ ) removes the ramified structure of clusters at  $E_n = 0.7$  eV, yielding elongated but compact clusters with smooth boundaries. The emergence of elongated clusters reveals an imbalance between attachment and detachment rates for in-plane bonds in x- and y-direction, respectively. This is understandable from the fact that, for  $\eta < 1$  the hopping rate  $r_{ij}$  [see Eq. (1)] of a particle with in-plane bonds in y-direction only is higher compared to particles with in-plane bonds in x-direction because at  $\eta < 1$  the inequality  $\eta E_n = E_n^y < E_n^x$  holds.

So far we have concentrated on the directly visible differences in the spatial configurations of individual clusters at low and high interaction energy at isotropic and strongly anisotropic interactions. One also observes an impact of interaction anisotropy ( $\eta < 1$ ) on the distribution of cluster sizes  $S$ . This is shown for the normalized cluster size distribution  $P(S)$  in Fig. 3. For isotropic interactions and  $E_n = 0.2$  eV,  $S$  is rather equally distributed around a mean value of  $S \approx 30$ . This peak vanishes for interaction anisotropies  $\eta < 0.4$  and  $P(S)$  becomes flat in the region  $S \geq 20$ . Instead,  $P(S)$  peaks at  $S < 5$  for  $\eta < 0.4$ , which reflects a mixture of a few large and many very small clusters. Thus, the interaction anisotropy leads to a completely different composition of cluster sizes in the system. The reduced amount of large clusters is due to the lowered interaction energy  $E_n^y$  of bonds in y-direction at  $\eta < 1$ . It follows that the detachment rate of particles with in-plane bonds in y-direction only increases as  $\eta$  is decreased. Consequently, less stable clusters are formed and at  $\theta = 0.05$  only a few clusters managed to surpass the critical cluster size to become stable. The situation is different at  $E_n = 0.7$  eV. Decreasing the anisotropy parameter from  $\eta = 1$  to  $\eta = 0.4$

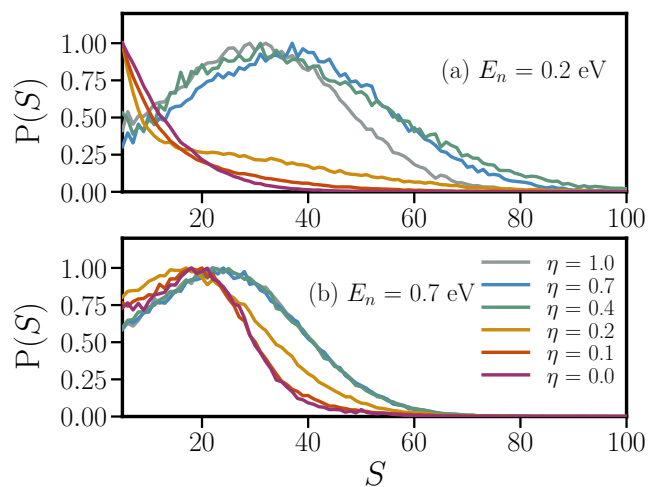


FIG. 3. (Color online) Distribution  $P(S)$  of cluster sizes  $S$  at interaction energy  $E_n = 0.2$  eV (a) and  $E_n = 0.7$  eV (b) and various values of the anisotropy parameter  $\eta$  ranging from isotropic conditions ( $\eta = 1$ ) to  $\eta = 0$  (no interaction energy for bonds along y-direction). Here and in the following figures, temperature  $T$  and adsorption rate  $F$  are chosen as in Fig. 2.

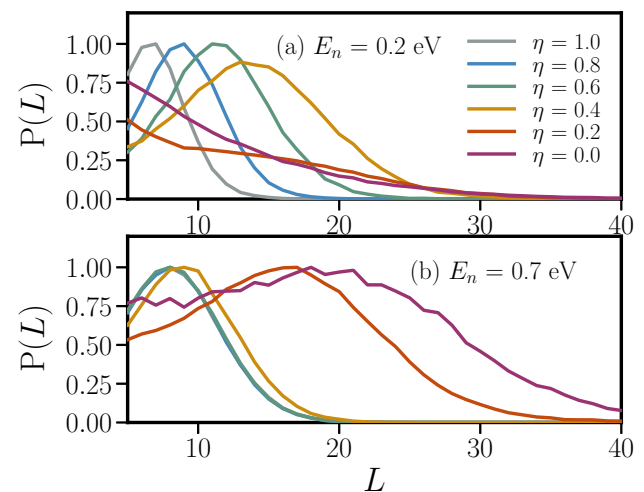


FIG. 4. (Color online) Distribution  $P(L)$  of cluster lengths  $L$  at  $E_n = 0.2$  eV (a) and  $E_n = 0.7$  eV (b) and various values of the anisotropy parameter  $\eta$ .

does not affect  $P(S)$ . Not until  $\eta < 0.4$ , the peak of  $P(S)$  shifts from  $S \approx 25$  to  $S \approx 20$  which only reflects a marginal change in the cluster size distribution. Further, the distribution becomes narrower and clusters of size  $S > 40$  vanish but the majority of clusters still has an intermediate size of  $S \approx 20$  that is quite similar to the value at isotropic growth conditions.

Additionally, the normalized cluster length distribution  $P(L)$  is shown in Fig. 4. At  $E_n = 0.2$  eV, the peak in the distribution  $P(L)$  is shifted to larger values of  $L$  and is slightly broadening as  $\eta$  is decreased from 1. This reflects the cluster elongation process, which continues up to  $\eta = 0.4$ . For stronger interaction anisotropies we

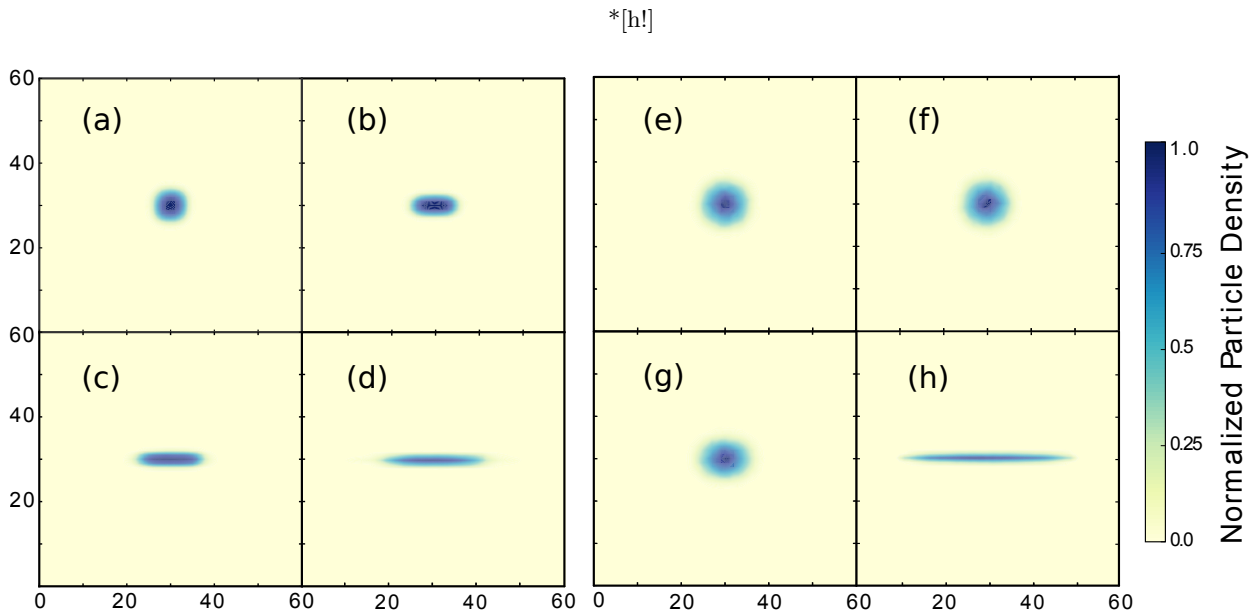


FIG. 5. (Color online) Average shapes of clusters of size  $S = 40$  for different values of the interaction anisotropy parameter  $\eta$  and the interaction energy  $E_n$ . The two values for  $E_n$  considered are  $E_n = 0.2$  eV (a-d) and  $E_n = 0.7$  eV (e-h). The parameter  $\eta$  is reduced from isotropic interactions ( $\eta = 1$ ) to 0.7, 0.4 and 0.1.

only observe a sharp peak at very small length  $L$ , consistent with the results in Fig. 3. At  $E_n = 0.7$  eV, the length distribution is not affected when  $\eta$  is decreased

from  $\eta = 1$  to  $\eta = 0.4$ . For  $\eta < 0.4$  the peak in  $P(L)$  is shifted towards larger lengths  $L$ . At the same time  $P(L)$  broadens.

\*

## 2. Average cluster shapes

We now focus in more detail on the response of the average cluster shapes upon variations of the anisotropy parameter  $\eta$ . To this end we present in Fig. 5 the average cluster shapes for fixed cluster size  $S = 40$  at  $E_n = 0.2$  [see Fig. 5 (a)-(d)] and  $E_n = 0.7$  eV [see Fig. 5 (e)-(h)] for four different values of the anisotropy parameter  $\eta$ . For  $\eta = 1$ , the average cluster shape is isotropic at both interaction energies,  $E_n = 0.2$  eV and  $E_n = 0.7$  eV, as expected. By decreasing  $\eta$  from 1 at  $E_n = 0.2$  eV, the average clusters become immediately elongated along the direction of stronger interaction energy, i.e. along the x-direction. Thus, already relatively weak interaction anisotropy ( $\eta = 0.7$ ) leads to anisotropic cluster shapes with growth preferred in x-direction. We conclude that at  $E_n = 0.2$  eV there is a gradual cluster shape transformation as function of  $\eta$  as soon as the regime of anisotropic interactions is entered ( $\eta < 1$ ). For strong interaction anisotropy, such as  $\eta = 0.1$ , we observe strongly elongated clusters whose average shape [see Fig. 5(d)] matches quite good with the individual clusters shown in Fig. 2(b).

At  $E_n = 0.7$  eV we encounter a different behavior of the cluster shape transformation. First, decreasing

$\eta$  from 1 to  $\eta = 0.4$  has essentially no impact on the initially isotropic shape. Second, at  $\eta = 0.1$ , the clusters are much stronger elongated compared to the case  $E_n = 0.2$  eV. This is in good agreement with the spatial configurations shown in Fig. 2(b) and (d). We conclude that there are two types of the cluster shape transformation, that is, gradual ( $E_n = 0.2$  eV) versus sharp ( $E_n = 0.7$  eV).

To further illustrate that the type of the cluster shape transformation depends on the interaction energy  $E_n$ , the spatial extension of clusters (of size  $S = 40$ ), namely the cluster length  $L$  and width  $W$  upon decreasing  $\eta$  from 1 are plotted in Fig. 6. At  $E_n = 0.2$  eV we observe an immediate splitting of  $L$  and  $W$ . This corresponds to anisotropic cluster growth where the cluster length and width grow at different rates, and thus, leads to the formation of elongated clusters. The smooth behavior of the splitting of  $L$  and  $W$  as function of  $\eta$  at  $E_n = 0.2$  eV confirms a gradual cluster shape transformation. In contrast, decreasing  $\eta$  from 1 at  $E_n = 0.7$  eV leaves  $L$  and  $W$  essentially identical up to  $\eta = 0.4$ . Only for  $\eta < 0.4$  we notice the splitting, which, in agreement with the results in Fig. 2 and Fig. 5, is also much stronger pronounced compared to  $E_n = 0.2$  eV and therefore the cluster shape transformation is sharp.

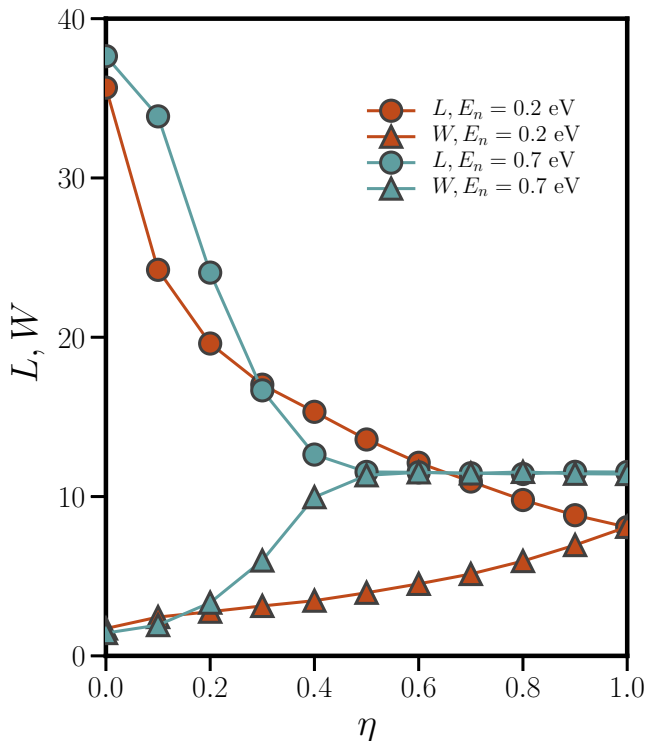


FIG. 6. (Color online) Evolution of cluster length  $L$  and width  $W$  at  $E_n = 0.2$  eV and  $E_n = 0.7$  eV as function of  $\eta$ . The considered clusters are of size  $S = 40$ . The evolution of  $L$  and  $W$  upon decrease of  $\eta$  from 1 confirms the gradual shape transformation at  $E_n = 0.2$  eV and the sharp shape transition at  $E_n = 0.7$  eV.

## B. Cluster shape properties - One-dimensional vs. two-dimensional cluster growth

### 1. Cluster length evolution

The results presented so far already demonstrate the impact of interaction anisotropy on the shape of clusters under non-equilibrium growth conditions. Now we focus on the evolution of cluster shapes during the cluster growth. To this end we plot in Fig. 7 the average cluster length  $L(S)$  as function of cluster size  $S$  for the two selected energies and different values of  $\eta$ . At  $E_n = 0.2$  eV and isotropic interactions ( $\eta = 1$ ),  $L(S)$  closely follows the solid black line that corresponds to isotropic cluster growth with  $L(S) = \sqrt{S}$ . In contrast, at  $E_n = 0.7$  eV and  $\eta = 1$  we observe small deviations from  $L(S) = \sqrt{S}$  because clusters are ramified [see Fig. 2(c)]. This results in a larger average spatial extension of clusters. However, the scaling  $L(S) \sim \sqrt{S}$  still holds which confirms the formation of isotropically shaped clusters also at  $E_n = 0.7$  eV.

As interaction anisotropy is switched on ( $\eta < 1$ ), we observe an immediate effect on the evolution of  $L(S)$  at  $E_n = 0.2$  eV, even at relatively weak interaction

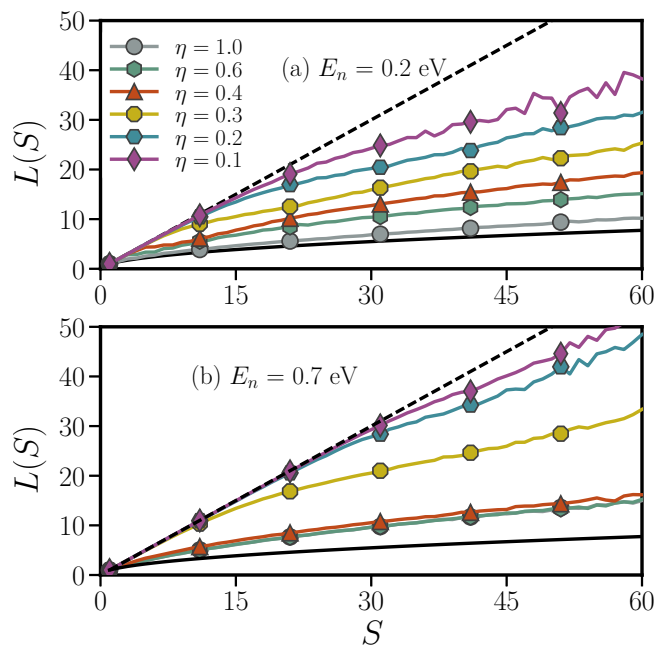


FIG. 7. (Color online) Average cluster length  $L(S)$  as function of cluster size  $S$  for interaction energy  $E_n = 0.2$  eV (a) and  $E_n = 0.7$  eV (b) and different values of  $\eta$ . The solid line represents  $L(S) = \sqrt{S}$ , while the dotted line corresponds to  $L(S) = S$

anisotropy. This is consistent with the previous results and confirms a gradual cluster shape transformation. Different from that, at  $E_n = 0.7$  eV, the  $L(S) \sim \sqrt{S}$  relations holds up to  $\eta \geq 0.4$ , which is consistent with the snapshots presented in Fig. 5 (f)-(h). This finding approves again that at high interaction energy ( $E_n = 0.7$  eV), weak interaction anisotropies ( $\eta \geq 0.4$ ) have far less impact on the cluster shape than at low interaction energies ( $E_n = 0.2$  eV).

As the interaction anisotropy becomes more pronounced, one finds, for both values of  $E_n$ , a transition from the scaling  $L(S) \sim \sqrt{S}$  to a linear relation  $L(S) = S$  as long as  $S$  remains small. The relation  $L(S) = S$  represents maximally elongated, one-dimensional clusters which grow only in the direction of the strong lateral bonds ("one-dimensional growth"). At  $E_n = 0.7$  eV and  $\eta = 0.1$ ,  $L(S)$  follows the one-dimensional growth line up to  $S \approx 30$ . While at  $E_n = 0.2$  eV and  $\eta = 0.1$ ,  $L(S)$  deviates from the  $L(S) = S$  already at around  $S \approx 10$ . Therefore, the one-dimensional growth is more robust at high interaction energies.

We conclude that in the presence of strongly anisotropic interactions, the initial stage of cluster growth appears to be one-dimensional with respect to particle attachment. This growth mode breaks down at a specific cluster length  $L_c$  which depends on  $E_n$  and  $\eta$ . The length  $L_c$ , is defined as the length of the cluster where  $|L(S) - S| \geq 1$  sets in upon increase of  $S$ . The value of  $L_c$  increases with increasing  $E_n$ , resulting in stronger

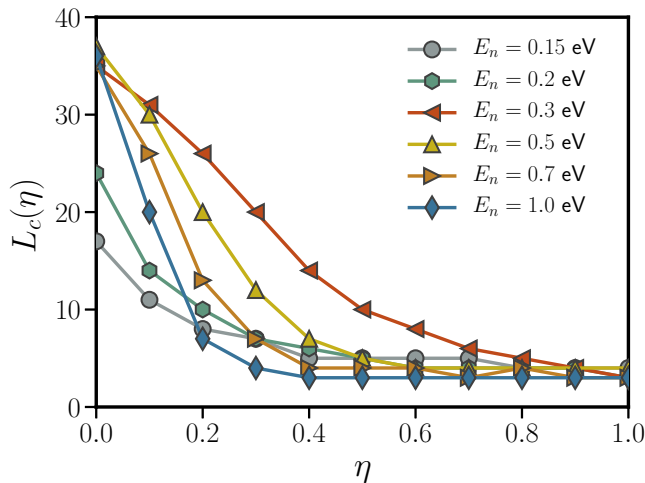


FIG. 8. (Color online) Critical length  $L_c(\eta)$  for various values of the interaction energy  $E_n$  as function of the anisotropy parameter  $\eta$ .

elongated clusters at high interaction energies.

### 2. The breakdown of one-dimensional cluster growth

In Fig. 8,  $L_c(\eta)$  is plotted for various interaction energies as function of  $\eta$ .

Irrespective of  $E_n$ , the function  $L_c(\eta)$  increases as  $\eta$  is decreased from 1 and converges to a finite value in the limit  $\eta \rightarrow 0$ . Specifically, in the range  $E_n \geq 0.3$  eV,  $L_c$  converges to very similar values  $L_c(0) = L_c^0 \approx 35$ . In contrast, at  $E_n < 0.3$  eV,  $L_c^0$  depends on  $E_n$ , e.g.  $L_c^0 \approx 25$  at  $E_n = 0.2$  eV and  $L_c^0 \approx 18$  at  $E_n = 0.15$  eV. We also see that, at  $E_n \leq 0.3$  eV, the increase of  $L_c$  as function of  $\eta$  is smooth and sets in already at weak interaction anisotropy. In contrast, at  $E_n > 0.3$  eV,  $L_c$  remains essentially unaffected by weak interaction anisotropy.

### 3. Transition to two-dimensional self-similar cluster growth

To better characterize the growth mode that follows the one-dimensional growth upon increase of the cluster size  $S$ , we calculate the average aspect ratio  $R(S) = L(S)/W(S)$ , where  $W(S)$  is the cluster width. An aspect ratio  $R$  that remains constant as function of cluster size  $S$  implies that the cluster growth is self-similar. This means, in other words, that  $L(S)$  and  $W(S)$  increase at constant rates. Figure 9 (a) shows  $R(S)$  for  $\eta \leq 0.4$  and different values of  $E_n$ . After an initial linear increase, corresponding to the region of one-dimensional cluster growth, the aspect ratio  $R(S)$  reaches a plateau and then remains constant as  $S$  increases. We call this saturation value  $R^{sat}$ . A saturation value  $R^{sat} = 1$  would correspond to isotropic self-similar growth without preferred growth direction [i.e.,  $L(S) = W(S)$ ]. For  $R^{sat} > 1$ , clus-

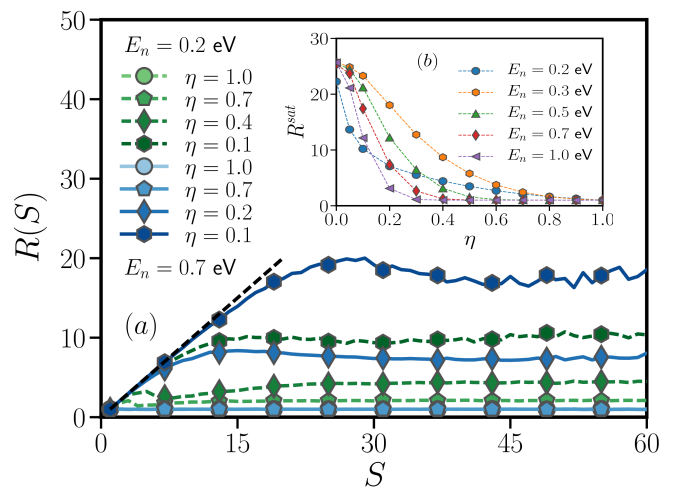


FIG. 9. (Color online) (a) Evolution of the average aspect ratio  $R(S) = L(S)/W(S)$  as function of cluster size  $S$  at  $E_n = 0.2$  eV (greens) and  $E_n = 0.7$  eV (blues) at different values of  $\eta$ . The black dotted line corresponds to  $R(S) = S$ . (b) Saturation value  $R^{sat}(\eta)$  for various interaction energies  $E_n$ .

ters are elongated [ $L(S) > W(S)$ ] but the growth is still self-similar. Such a plateau exists for all considered combinations of  $E_n$  and  $\eta$ . Only the actual value of  $R^{sat}$  and the cluster size  $S$ , where the plateau is reached, depend specifically on  $E_n$  and  $\eta$ .

In addition,  $R^{sat}$  is plotted for various  $E_n$  as function of  $\eta$  in Fig. 9 (b). For  $E_n \geq 0.3$  eV,  $R^{sat}$  converges to similar values as  $\eta \rightarrow 0$ . The onset of anisotropic self-similar growth ( $R^{sat} > 1$ ) is shifted to smaller values of  $\eta$  for increasing  $E_n$ . Furthermore, for  $E_n < 0.3$  eV,  $R^{sat}$  is lower compared to  $R^{sat} \approx 25$  as for  $E_n \geq 0.3$  eV.

### C. Role of the critical island size $i^*$

A major observation in presence of anisotropic interactions ( $\eta < 1$ ) is that, depending on the interaction energy  $E_n$ , there exist two types of cluster shape transformations. It turns out that this can be explained by properties of the isotropic reference systems ( $\eta = 1$ ). To this end, we now take a closer look at the critical island size  $i^*$  at  $\eta = 1$  as function of interaction energy  $E_n$ .

For this purpose, the critical island density  $\rho_N^c$  is plotted as function of  $E_n$  for the isotropically interacting reference systems ( $\eta = 1$ ) in Fig. 10. We recall that  $\rho_N^c$  scales  $\sim (D_0(T)/F)^{-\chi}$  [with  $\chi = i^*/(i^* + 2)$ ]. From Fig. 10 it is seen that  $\rho_N^c$  increases as the interaction energy is increased from  $E_n = 0.1$  eV to  $E_n = 0.3$  eV, but saturates in the range  $E_n > 0.3$  eV. Since we do not change the temperature  $T$  and adsorption rate  $F$ , it follows from the known scaling of  $\rho_N^c$  [46, 48, 50, 51] that  $i^*$  has to be identical for all  $E_n > 0.3$  eV. In this regime, the critical island size therefore is  $i^* = 1$ , which corresponds to conditions where bonds are *irreversible*.

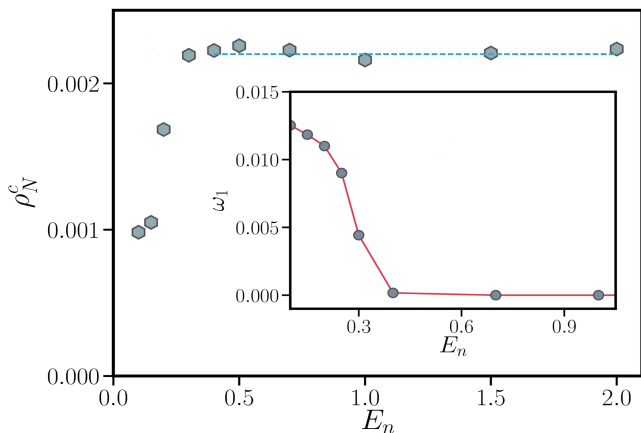


FIG. 10. (Color online) Critical island density  $\rho_N^c$  for different in-plane interaction energies  $E_n$  in the (isotropic) reference system. The inset shows the detachment ratio  $\omega_1$  as function of  $E_n$ .

This conclusion is confirmed by the analysis of  $\omega_1(E_n)$  [see Eq. (9)] at  $\eta = 1$  (see the inset of Fig. 10). Consistent with the analysis so far,  $\omega_1 = 0$  for  $E_n > 0.3$  eV, which means absence of particle detachment (bonds are *irreversible*). In other words, already dimers form stable clusters and  $i^* = 1$ . As  $E_n$  is decreased towards lower values,  $\omega_1$  becomes nonzero, which means that bonds become *reversible* (particles can break bonds and detach from clusters). Consequently, one enters the regime of  $i^* > 1$ . We conclude that, coming from high interaction energies, there is a transition from *irreversible* to *reversible* bonds at  $E_n \approx 0.3$  eV. This observation allows to explain the type and the onset of the cluster shape transformation in presence of anisotropic interactions ( $\eta < 1$ ). We can distinguish between three different scenarios.

### 1. Interaction energy $E_n > 0.3$ eV and $\eta = 1$

In this case, bonds are *irreversible* in x- and y-direction and consequently, cluster growth is isotropic for any  $E_n > 0.3$  eV (see inset of Fig. 9 at  $\eta = 1$  where  $R^{sat} = 1$  at  $\eta = 1$ ).

### 2. Interaction energy $E_n > 0.3$ eV and $\eta < 1$

In this situation, bonds in x-direction are *irreversible* and as long as  $E_n^y = \eta E_n > 0.3$ , also bonds in y-direction are *irreversible* and therefore, cluster growth is isotropic even for  $\eta < 1$  (as long as  $E_n^y > 0.3$  eV). However, as soon as the regime  $E_n^y = \eta E_n < 0.3$  is entered by increasing the strength of the interaction anisotropy, bonds in y-direction become *reversible* while bonds in x-direction remain *irreversible*. Anisotropic cluster growth sets in at the value of  $\eta$  that leads  $E_n^y \leq 0.3$  eV. At  $E_n = 0.5$  eV, we find the onset of the transformation at  $\eta = 0.6$ , which

corresponds to  $E_n^y = 0.3$  eV, consistent with the transition from *irreversible* to *reversible* bonds. The same holds at  $E_n = 1.0$  eV, where we find the onset at  $\eta = 0.3$ , which again corresponds to  $E_n^y = 0.3$  eV for bonds along the y-direction. This explains, depending on  $E_n$ , the sharp cluster shape transformation and the precise value  $\eta$  where it sets in.

### 3. Interaction energy $E_n < 0.3$ eV and $\eta \leq 1$

Here, bonds in both, x- and y-direction are *reversible*. At  $\eta = 1$ , cluster growth is isotropic because there is no imbalance between bond strengths,  $E_n^x = E_n^y$ . In contrast to case 2., clusters become elongated for any  $\eta < 1$  because we are always in the regime of *reversible* bonds ( $E_n^y < 0.3$  for all  $\eta$ ). Even though bonds in x-direction are *reversible*, the detachment rate for bonds in y-direction is higher at  $\eta < 1$ . Therefore, clusters growth is anisotropic with growth preferred in x-direction (despite the fact that also bonds in x-direction are *reversible*). Different from case 2., the cluster shape transformation here is gradual because we are always in the regime where bonds are *reversible*.

Moreover, we can also explain why both,  $L_c$  and  $R^{sat}$  converge to similar values for  $E_n \geq 0.3$  as  $\eta \rightarrow 0$  (see Fig. 8 and Fig. 9). In the latter case,  $E_n^y = 0$ . Therefore, all of the systems are identical in the sense that bonds in x-direction are *irreversible* while bonds in y-direction are *reversible*. The hopping rate for particles with bonds in y-direction only is the same as the rate for free diffusion,  $r_{ij} \sim \exp(-\beta E_d)$ . The reason for this is that at  $\eta = 0$  there is no contribution to the activation energy barrier  $\Delta E$  from in-plane bonds in this direction. Consequently,  $L_c(0)$  and  $R^{sat}(0)$  is practically the same for  $E_n \geq 0.3$  eV.

## D. The anisotropic stochastic Eden growth model

So far we investigated cluster growth within the event-driven kMC simulation setup where adsorption, nucleation, attachment, detachment and diffusion processes of particles on the substrate are included. We now turn to the much simpler anisotropic Eden model for cluster growth (see Sec. II, B) where anisotropy of lateral bonds is induced by an imbalance of attachment probabilities as described in Eq. (6). One main difference to the kMC model is that diffusion processes are absent in the Eden model, where the cluster growth is only determined by the attachment probabilities of boundary sites. Our key question is whether this minimal model still contains sufficient information to reproduce the clusters obtained in the kMC simulations for various anisotropic growth conditions.

For this purpose, we plot in Fig. 11 the cluster length  $L(S)$  for clusters obtained from both, kMC simulations

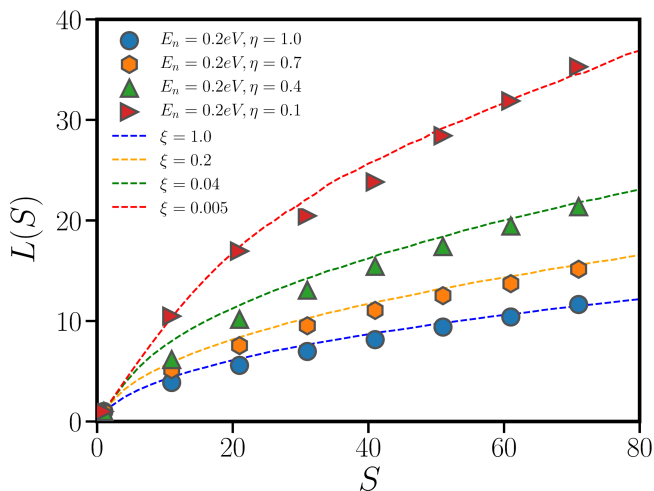


FIG. 11. (Color online) Comparison of the cluster length evolution between clusters obtained from kinetic Monte-Carlo simulations (at  $E_n = 0.2$  eV and different values of  $\eta$ ) with clusters obtained from the stochastic Eden model at different ratios  $\xi$  of the attachment probability in x- and y-direction, respectively.

at  $E_n = 0.2$  eV and simulations of the Eden model. This value for  $E_n$  is chosen because it produces compact clusters at  $\eta = 1$ . The good agreement for the isotropic case ( $\eta = \xi = 1$ ) is expected since there is no imbalance between attachment and detachment rates for the x- and y-direction. More interesting is the matching of both models in the regime where anisotropic interactions are present. Here, the anisotropy parameter  $\xi$  for the attachment probabilities in the Eden model [see Eq. (6)] has been used as a fitting parameter to reproduce the kMC results. The Eden model does not only correctly describe the cluster length evolution  $L(S)$ , but also gives the correct critical lengths  $L_c$  and the aspect ratio  $R^{sat}$  in the self-similar growth regime. This is shown in Fig. 12 (a) and 12 (b), respectively.

The agreement between the two approaches suggests that the isotropic diffusion of free particles does not play a crucial role for the cluster formation process in presence of anisotropic in-plane bonds. Rather, it is indicated that only the rates for attachment and detachment determine the cluster shape. Therefore, we expect that a more detailed analysis of attachment and detachment rates will help to better understand the resulting cluster shapes under non-equilibrium growth conditions.

#### IV. CONCLUSIONS

Using event-driven kMC simulation on a square-lattice we have studied the effect of anisotropic nearest-neighbor interactions in the sub-monolayer growth regime. Our model assumes a spherical particle shape. Anisotropy is introduced by reducing the interaction energy of in-plane bonds along the y-direction by a factor  $\eta$  relative

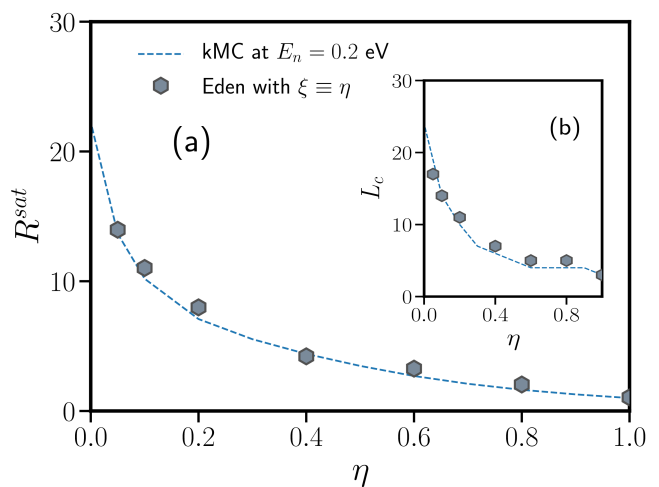


FIG. 12. (Color online) (a) Saturation value of the aspect ratio  $R^{sat}$  and (b) the critical length  $L_c$  of clusters obtained from kinetic Monte-Carlo simulations and the Eden model. The in-plane interaction energy in kMC simulations is  $E_n = 0.2$  eV. The anisotropy parameter  $\eta \in [0, 1]$  and  $\xi$  is modified such that it fits the kMC results.

to the interaction energy in x-direction. By varying the interaction energy and the anisotropy parameter we have analyzed in detail the resulting clusters in presence of anisotropic interactions.

As expected, anisotropic interactions lead to non-spherical (elongated) cluster shapes, as we have shown explicitly by corresponding snapshots. Furthermore, cluster size distributions show that, for increasing interaction anisotropy, clusters become smaller. This effect is the more pronounced the smaller  $E_n$ .

A detailed analysis of cluster shapes as function of  $\eta$  reveals two different types of cluster shape transformation. At low interaction energy, the transformation from isotropic to elongated clusters is gradual. In contrast, it is sharp at high interaction energies. Moreover, for strong interaction anisotropy, the early stage of cluster growth appears to be one-dimensional with particle attachment along the direction of strong bonds only. This growth mode breaks down at a critical length. From analyzing the aspect ratio we identify the subsequent self-similar growth mode.

Interestingly, we have found that the critical island density and detachment ratio in the isotropic reference system help to explain the properties of the cluster shape transformation in the anisotropic case. Furthermore, the comparison with the reference systems also explains the value of the anisotropy parameter where the transformation from isotropic to elongated cluster shapes sets in.

In addition to kMC simulations, we have also employed an anisotropic version of the Eden model where diffusion processes are neglected. In this context, we have used the anisotropy parameter, that controls the attachment probabilities, as a fitting parameter. By this it is indeed possible to reproduce main features of the cluster growth

observed in the kMC simulations. In particular, we find good agreement in the cluster length evolution, the critical length and the saturation value of the aspect ratio.

The good agreement between results from kMC simulations and the Eden model suggests that attachment (rather than diffusion) is the dominant mechanism in determining cluster shapes. Therefore it may be worth to further investigate, on a very fundamental level, attachment as well as detachment rates to gain a deeper understanding of the cluster shape transformations. We also mention two possible extensions of the kMC simulations presented here. First, by appropriate setting of the values for the anisotropy parameter in the kMC setup, our

model allows to study the effect of dipole-dipole interactions among particles. By this one could approach experimentally relevant systems that have already been studied [34, 35]. A second future direction would be to explore, based on our model, the multilayer growth regime. Investigations in these directions are in progress.

## ACKNOWLEDGMENTS

This work was supported by the Deutsche Forschungsgemeinschaft within the framework of the Collaborative Research Center CRC 951 (project A7). We also thank J. Dzubiella and M. Miletic for fruitful discussions.

- 
- [1] S. Blumstengel, H. Glowatzki, S. Sadofev, N. Koch, S. Kowarik, J. P. Rabe, and F. Henneberger, *Phys. Chem. Chem. Phys.* **12**, 11642 (2010).
- [2] P. Cao, K. Xu, J. O. Varghese, and J. R. Heath, *J. Am. Chem. Soc.* **133**, 2334 (2011)
- [3] H. Ma, O. Acton, D. O. Hutchins, N. Cernetic, and A. K.-Y. Jen, *Phys. Chem. Chem. Phys.* **14**, 14110 (2012).
- [4] R. Nötzel, Z. Niu, M. Ramsteiner, H. P. Schönherr, A. Trappert, L. Däweritz, and K. H. Ploog, *Nature*, **392**, 56-59 (1998)
- [5] L. Bao, W. Wang, N. Meyer, Y. Liu, C. Zhang, K. Wang, P. Ai, and F. Xiu, *Sci. Rep.* **3**, 2391 (2013)
- [6] I. Božović, X. He, J. Wu, and A. T. Bollinger, *Nature* **536**, 309-311 (2016)
- [7] L. Sapienza, J. Liu, J. D. Song, S. Fält, W. Wegscheider, A. Badolato, and K. Srinivasan, *Sci. Rep.* **7**, 6205 (2017)
- [8] K. Wang, Y. Gu, H. F. Zhou, L. Y. Zhang, C. Z. Kang, M. J. Wu, W. W. Pan, P. F. Lu, Q. Gong, and S. M. Wang, *Sci. Rep.* **4**, 5449 (2014)
- [9] J. D. Albar, A. Summerfield, T. S. Cheng, A. Davies, E. F. Smith, A. N. Khlobystov, C. J. Mellor, T. Taniguchi, K. Watanabe, C. T. Foxon, L. Eaves, P. H. Beton, and S. V. Novikov, *Sci. Rep.* **7**, 6598 (2017)
- [10] H. S. Wang, D. Eissler, W. Dietsche, A. Fischer, and K. Ploog, *J. Cryst. Growth* **127**, 665-658 (1993)
- [11] Y. Wang, Y. N. Sheng, W. Ge, J. Wang, L. L. Chang, J. Xie, J. Ma, and J. Xu, *J. Cryst. Growth* **175**, 1289-1293 (1997)
- [12] J. C. Moore, K. A. Cooper, J. Xie, H. Morkoc and A. A. Baski, *Proceedings of the SPIE*, **6121**, 160-165 (2006)
- [13] N. P. Kobayashi, T. R. Ramachandran, P. Chen, and A. Madhukar, *Appl. Phys. Lett.* **68**, 3299 (1996)
- [14] A. Brazdeikis, U. O. Karlsson, A. S. Flodström, *Thin Solid Films* **281-282**, 57-59 (1996)
- [15] G. W. Brown, M. E. Hawley, C. D. Theis, J. Yeh, and D. G. Schlom, *Journal of Electroceramics*, **4**, 351-356 (2000)
- [16] J. D. Benson, L. A. Almeida, M. W. Carmody, D. D. Edwall, J. K. Markunas, R. N. Jacobs, M. Martinka, and U. Lee, *Journal of Electronic Materials*, **36**, 949-957 (2007)
- [17] Ph. Lavalle, C. Gergely, F. J. G. Cuisinier, G. Decher, P. Schaaf, J. C. Voegel, and C. Picart, *Macromolecules*, **35**, 4458-4465 (2002)
- [18] F. S. Khokhar, G. Hlawacek, R. van Gastel, H. J.W. Zandvliet, C. Teichert, and B. Poelsema, *Surf. Sci.* **606**, 475-480 (2012)
- [19] L. Huang, S. Jay Chey, and J.H. Weaver, *Surf. Sci.* **416**, 1101-1106 (1998)
- [20] H. Hirayama, *Surf. Sci.* **603**, 1492-1497 (2009)
- [21] A. Pal, J. C. Mahato, B. N. Dev, and D. K. Goswami, *Appl. Mater. Interfaces*, **5**, 9517-9521 (2013)
- [22] M. Miyazaki, and H. Hirayama, *Surf. Sci.* **602**, 276-282 (2008)
- [23] D. Placencia, W. Wang, R. C. Shallcross, K. W. Nebesny, M. Brumbach, and N. R. Armstrong, *Adv. Funct. Mater.* **19**, 1913 (2009)
- [24] F. J. Meyer zu Heringdorf, M. C. Reuter, and R. M. Tromp, *Nature* **412**, 517 (2001)
- [25] F. S. Khokhar, G. Hlawacek, R. van Gastel, H. J. W. Zandvliet, C. Teichert, and B. Poelsema, *Surf. Sci.* **606**, 475 (2012)
- [26] J. A. Venables, J. Derrien, and A. P. Janssen, *Surf. Sci.* **95**, 411-430 (1980)
- [27] M. Hanbücken, M. Futamoto, and J. A. Venables, *Surf. Sci.* **147**, 433-450 (1984)
- [28] M. Horn-von Hoegen, T. Schmidt, M. Henzler, G. Meyer, D. Winau, and K. H. Rieder, *Surf. Sci.* **331-333**, 575-579 (1995)
- [29] O. Schuler, X. Wallart, and F. Mollot, *Journal of Crystal Growth*, **201**, 280-283 (1999)
- [30] A. A. Khosroabadi, D. L. Matz, P. Gangopadhyay, J. E. Pemberton, and R. A. Norwood, *J. Phys. Chem. C* **118**, 18027 (2014)
- [31] M. Hanbeken, and H. Neddermeyer, *Surf. Sci.* **114**, 563-573 (1982)
- [32] S. Bommel, N. Kleppmann, C. Weber, P. Schäfer, J. Novak, S. V. Roth, F. Schreiber, S. H. L. Klapp, and

- S. Kowarik, *Nat. Comm.* **5**, 5388 (2014)
- [33] A. Hinderhofer, A. Gerlach, S. Kowarik, F. Zontone, J. Krug, and F. Schreiber, *Europhys. Lett.* **91**, 56002 (2010)
- [34] M. Sparenberg, A. Zykov, P. Beyer, L. Pithan, C. Weber, Y. Garmshausen, F. Carlà, S. Hecht, S. Blumstengel, F. Henneberger, and S. Kowarik, *Phys. Chem. Chem. Phys.*, **16**, 26084, (2014)
- [35] F. Della Sala, S. Blumstengel, and F. Henneberger, *Phys. Rev. Lett.* **107**, 146401 (2011)
- [36] A. Zykov, S. Bommel, C. Wolf, L. Pithan, C. Weber, P. Beyer, G. Santoro, J. P. Rabe, and S. Kowarik, *J. Chem. Phys.* **146**, 052803 (2017)
- [37] P. Beyer et al., *ACS Appl. Mater. Interfaces*, **6**, 2148421493, (2014)
- [38] C. Frank, J. Novák, R. Banerjee, A. Gerlach, F. Schreiber, A. Vorobiev, and S. Kowarik, *Phys. Rev. B*, **90**, 045410 (2014)
- [39] S. Kowarik, *J. Phys.: Condens. Matter*, **29** 043003 (2017)
- [40] L. Pithan, P. Beyer, L. Bogula, A. Zykov, P. Schfer, J. Rawle, C. Nicklin, A. Opitz, and S. Kowarik, *Advanced Materials*, **29**, 1521 (2017)
- [41] J. P. Bucher, E. Hahn, P. Ferbabdez, C. Massobrio, and K. Kern, *Europhys. Lett.*, **27** (6), pp. 473-478 (1994)
- [42] R. Ferrando, F. Hontinfinde, and A. C. Levi, *Phys. Rev. B* **56**, R4406(R) (1997)
- [43] Z. J. Liu, and Y. G. Shen, *J. Vac. Sci. Technol. A* **23**, 177 (2005)
- [44] R. Ferrando, *Phys. Rev. Lett.* **76**, 4195 (1996)
- [45] R. Ferrando, F. Hontinfinde, and A. C. Levi, *Surf. Sci.* **366**, 306 (1996)
- [46] K. A. Jackson, *J. Cryst. Growth*, **1**, 13-18 (1969)
- [47] F. Gibou, C. Ratsch, and R. E. Caflisch, *Phys. Rev. B* **67**, 155403 (2003)
- [48] J. G. Amar, M. N. Popescu, and F. Family, *Phys. Rev. Lett.* **86**, 3092 (2001).
- [49] J. A. Venables, R. Persaud, F. L. Metcalfe, R. H. Milne, and M. Azim, *J. Phys. Chem. Solids* **55**, 955-964 (1994)
- [50] J. G. Amar, F. Family, M. N. Popescu, *Computer Physics Communications* **146**, 1-8 (2002)
- [51] M. Körner, M. Einax, P. Maass, *Phys. Rev. B* **82**, 201401(R) (2010)
- [52] M. Körner, M. Einax, P. Maass, *Phys. Rev. B* **86**, 085403 (2012)
- [53] J. G. Amar, and M. N. Popescu, *Phys. Rev. B* **69**, 033401 (204)
- [54] Y. Han, M. Li, J. W. Evans, *J. Chem. Phys.* **145**, 211911 (2016)
- [55] J. W. Evans et al., *Surf. Sci. Rep.* **61**, 1 (2006)
- [56] J. G. Amar, and F. Family, *Phys. Rev. Lett.* **74**, 2066 (1995)
- [57] J. A. Venables, *Philos. Mag.* **27**, 697-738 (1973)
- [58] J. A. Nieminen, and K. Kaski, *Phys. Rev. A* **40** 2088 (1989)
- [59] J. A. Nieminen, and K. Kaski, *Phys. Rev. A* **40** 2096 (1989)
- [60] J. G. Amar, F. Family, and P. M. Lam, *Phys. Rev. B* **50** 8781 (1994)
- [61] N. Kleppmann, and S. H. L. Klapp, *Phys. Rev. B* **91**, 045436 (2015)
- [62] M. Haran, J. E. Goose, N. P. Clote, and P. Clancy, *Langmuir* **23**, 4897 (2007)
- [63] S. F. Hopp, and A. Heuer, *J. Chem. Phys.* **133**, 204101 (2010)
- [64] P. K. Jana, and A. Heuer, *J. Chem. Phys.* **138**, 124708 (2013).
- [65] P. Rotter, B. A. J. Lechner, A. Morherr, D. M. Chisnall, D. J. Ward, A. P. Jardine, J. Ellis, W. Allison, B. Eckhardt, and G. Witte, *Nature Materials* **15**, 397400 (2016)
- [66] N. Kleppmann, and S. H. L. Klapp, *J. Chem. Phys.* **142**, 064701 (2015)
- [67] N. Kleppmann, and S. H. L. Klapp, *Phys. Rev. B* **94**, 241404(R) (2016)
- [68] K. Palczynski and J. Dzubiella, *J. Phys. Chem. C* **118**, 26368 (2014).
- [69] K. Palczynski, P. Herrmann, G. Heimel, and J. Dzubiella, *Phys. Chem. Chem. Phys.* **18**, 25329-25341 (2016)
- [70] K. Palczynski, G. Heimel, J. Heyda, and J. Dzubiella, *Crystal Growth and Design* **14**, 3791 (2014)
- [71] J. A. Venables, G. D. Spiller, and M. Hanbucken, *Rep. Prog. Phys.* **47**, 399 (1984)
- [72] T. A. Witten, Jr., and L. M. Sander, *Phys. Rev. Lett.* **47**, 1400 (1981)
- [73] T. A. Witten, and L. M. Sander, *Phys. Rev. B* **27**, 5686 (1983)
- [74] P. Meakin, *Phys. Rev. Lett.* **51**, 1119 (1983)
- [75] T. Vicsek, *Phys. Rev. Lett.* **53**, 2281 (1984)
- [76] G. Daccord, J. Nittmann, and H. E. Stanley, *Phys. Rev. Lett.* **56**, 336 (1986)
- [77] M. Eden, *Proceedings of Fourth Berkeley Symposium on Mathematics, Statistics, and Probability*. 4. Berkeley: University of California Press. pp. 223239 (1961)
- [78] M. Kolb, R. Botet, and R. Jullien, *Phys. Rev. Lett.* **51**, 1123-1126 (1983)
- [79] Z. Yao, and M. O. de la Cruz, *J. Phys. Chem. B* **120**, 59605965 (2016)
- [80] R. Jullien, and R. Botet, *J. Phys. A* **21**, 3501 (1988)
- [81] P. Meakin, *J. Phys. A* **22**
- [82] R. L. Smith, and S. D. Collins, *Phys. Rev. A* **39**, 5409 (1989)
- [83] A. C. Aristotelous, and R. Durrett, *Exp Math.* **23**, 465474 (2014)
- [84] M. Oettel, M. Klopotek, M. Dixit, E. Empting, T. Schilling, and H. Hansen-Goos, *J. Chem. Phys.* **145**, 074902 (2016)
- [85] M. Klopotek, H. Hansen-Goos, M. Dixit, T. Schilling, F. Schreiber, and M. Oettel, *J. Chem. Phys.* **146**, 084903 (2017)
- [86] J. E. Goose, E. L. First, and P. Clancy, *Phys. Rev. B* **81**, 205310 (2010)
- [87] G. Hlawacek, P. Puschnig, P. Frank, A. Winkler, C. Ambrosch-Draxl, and C. Teichert, *Science* **321**, 108 (2008)
- [88] S. Clarke and D. D. Vvedensky, *J. Appl. Phys.* **63**, 2272 (1988)
- [89] T. J. Oliveira, and F. D. A. Araújo Reis, *Phys. Rev. B* **87**, 235430 (2013)